

GT2011-453' \$

CONVECTIVE AND ABSOLUTE INSTABILITIES IN REACTING BLUFF BODY WAKES

Benjamin Emerson, Julia Lundrigan, Jacqueline O'Connor, David Noble, Tim Lieuwen

Ben T Zinn Combustion Laboratory
Department of Aerospace Engineering
Georgia Institute of Technology
tim.lieuwen@aerospace.gatech.edu

ABSTRACT

This paper describes the variation of bluff body wake structure with flame density ratio. It is known that the bluff body flow structure at “high” and “low” flame density ratios is fundamentally different, being dominated by the convectively unstable shear layers or absolutely unstable Von Karman vortex street, respectively. This paper characterizes the aforementioned transition and shows that the bifurcation in flow behavior does not occur abruptly at some ρ_u/ρ_b value. Rather, there exists a range of transitional density ratios at which the flow exists intermittently in both flow states, abruptly shifting back and forth between the two. The fraction of time that the flow spends in either state is a monotonic function of ρ_u/ρ_b . This behavior is to be contrasted with lower Reynolds number, laminar flow problems where the convective/absolute instability transition occurs at a well defined value of bifurcation parameter. With this distinction in mind, however, this paper also shows that local parallel stability analyses developed for laminar base wake flows can capture many of the observed flow dependencies. These results have important implications on the dynamics of high Reynolds number, vitiated flows, where typical parameter values fall into the highly intermittent flow regime characterized in this study. This suggests that such flows exhibit two co-existing dynamical states, intermittently jumping between the two.

NOMENCLATURE

A	=	flow cross-sectional area
D	=	bluff body diameter
\dot{m}	=	mass flowrate
Re	=	Reynold's number, $U_{lip}D/\nu$
St_D	=	Strouhal number, fD/U_{lip}
T	=	temperature
U	=	time-averaged axial velocity
c	=	modal wave propagation speed
f	=	frequency, Hz

k	=	wavenumber
s	=	parameter specifying varicose (-1) vs. sinuous (1) mode
t	=	time
v	=	instantaneous transverse velocity

GREEK CHARACTERS

β	=	backflow ratio, $-U(y=0)/U(y=\infty)$
ζ_L	=	lower flame edge position
ζ_U	=	upper flame edge position
ν	=	kinematic viscosity
ρ	=	gas density
ρ_f	=	correlation coefficient between sine fit and original time signal
$\rho_{U,L}$	=	correlation coefficient between upper and lower flame edge positions
ρ_t	=	correlation coefficient threshold
ϕ	=	equivalence ratio
ω	=	frequency, rad/s

SUBSCRIPTS

0	=	zero group velocity
b	=	burned
i	=	imaginary component
lip	=	bluff body trailing edge lip
max	=	maximum
ref	=	reference velocity
u	=	unburned

SUPERSCRIPTS

'	=	unsteady component
---	---	--------------------

BACKGROUND

Bluff bodies are a common mode of flame stabilization in a variety of practical combustion devices [2]. The unsteady flow fields in bluff body flows, both with and without the presence of

combustion, are often dominated by large scale coherent structures, embedded upon a background of acoustic waves and broadband fine scale turbulence. These large scale structures play important roles in such processes as combustion instabilities, mixing and entrainment, flashback, and blowoff. The objective of this study is to experimentally characterize the role of flame density ratio upon the appearance and characteristics of these structures in a reacting bluff body wake.

These large scale structures arise because of underlying hydrodynamic instabilities of the flow field [3]. The concepts of *convective* and *absolute* stability of the base flow [4-6] upon which these flow disturbances are initiated, and subsequently amplified or damped, will play an important role in the subsequent discussions, so it is helpful to review a few key concepts. In an unstable flow, disturbances are amplified. These amplified disturbances in a convectively unstable flow are swept downstream so that the response at any fixed spatial point eventually tends toward zero. In contrast, perturbations in absolutely unstable flows increase in amplitude at a fixed spatial location, even as the actual flow particles are convected downstream [7].

The implications of this absolute/convective instability distinction are important. A “convectively unstable” flow acts an *amplifier*, in that a disturbance created at some point grows in amplitude as it is convected out of the system. However, the oscillations are not self-excited but require a constant disturbance source to persist. In any real situation, there are a variety of background disturbances, such as broadband turbulence and harmonic acoustic disturbances, which provide this consistent source of excitation. The flow then selectively filters these background disturbances. For example, in convectively unstable shear flows, the spectrum shows a distributed peak around a frequency associated with the most rapidly amplified mode, a frequency that can be predicted from linear instability theory [8]. When such systems are forced by external disturbances, such as acoustic waves, these disturbances are easily discerned in the system response.

An absolutely unstable system is an *oscillator* – it exhibits intrinsic, self-excited oscillations and does not require external disturbances to persist. In such a self-excited system, the amplitude grows before saturating into a limit cycle oscillation. Moreover, the spectrum of oscillations shows a narrowband peak associated with this natural frequency. When externally forced, the limit cycle behavior may be insensitive to the external forcing, unless the amplitude is high enough that the phenomenon of “lock-in” occurs [9-10]. In other words, in a convectively unstable flow, there is a monotonic relationship between forcing amplitude and system response, while in an absolutely unstable system, the limit cycle oscillations persist despite this forcing, except at high forcing levels. These distinctions are important in combustion instability problems, where vortical structures excited by acoustic waves play important roles in the feedback mechanism. In one case, low amplitude acoustic excitation will induce a proportional response while in the other it may not. In turn, this has

important implications on which type of flow instabilities can be involved in linear combustion instability mechanisms.

As shown in Figure 1, there are two key flow features downstream of the bluff body, the separating free shear layer [11] and the wake, both of which strongly influence the flame. These two flow features are discussed further next.

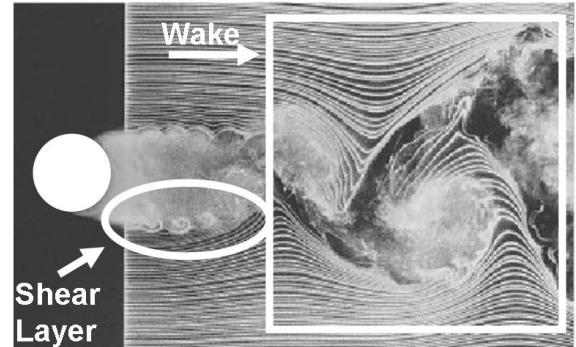


Figure 1. Key features of non-reacting flow past a bluff body at $Re = 10,000$. Reproduced from Prasad and Williamson [12]

The separated shear layer evolves in a similar manner to a mixing layer given a sufficiently long recirculation zone length. It is *convectively* unstable due to the Kelvin-Helmholtz mechanism for $Re_D > \sim 1200$, leading to shear layer rollup into tightly concentrated vorticity. In most practical configurations, the flame lies nearly parallel to the flow and, thus, almost directly in the bluff body shear layer for practical high velocity flows. The separating vorticity sheet on both sides of the bluff body rolls up, which induces a flow field that wraps the flame around these regions of intense vorticity.

In non-reacting flows, the bluff body wake is absolutely unstable, and characterized by large scale, asymmetric vortex shedding [13] known as the Von Karman vortex street. This instability has a characteristic frequency of [12]

$$f_{BVK} = St_D \cdot \frac{U_\infty}{D} \quad (1)$$

where St_D is the Strouhal number. For circular cylinders, St_D is independent of Reynolds number ($St_D = 0.21$) in the turbulent shear layer, laminar boundary layer regime, $\sim 1000 < Re_D < \sim 200,000$ [14]. Above $Re_D = \sim 200,000$, the boundary layer starts to transition to turbulence and there are some indications that this Strouhal number value changes [15-16].

This Strouhal number value is a function of bluff body shape [10]. In particular, St_D is lower for “bluffer” bodies, i.e., those with higher drag and wider wakes [17]. For example, $St_D \sim 0.18$ for a 90 degree “v-gutter” and drops to 0.13 for a sharp edge, vertical flat plate [18]. Roshko suggests that St_D fundamentally scales with the wake width [17, 19] and, therefore, care must be applied in inferring Strouhal numbers

from one bluff body shape to another. For example, flow separation is retarded for circular bluff bodies when the boundary layer transitions to turbulence, implying a reduction in wake width and turbulent vortex roll-up [20]. In contrast, the flow separation point would not move in bluff bodies with sharp separation points.

There is a large literature on the effects of wake heating [19-22], splitter plates [11], and wake bleeding on the absolute stability characteristics of the wake. Of most interest to this study are analyses showing that a sufficiently hot wake relative to the free stream eliminates the absolute instability of the wake, so that its dynamics are then controlled by the convectively unstable shear layers. For example, Yu [21] and Monkewitz [7, 21] reported the results of a parallel stability analysis in an unconfined domain. In this analysis, they expand the equations of fluid motion in normal modes as.

$$q' = \text{real}\{\hat{q} \exp[i(kx - \omega t)]\} \quad (2)$$

where q' is any general flow perturbation. These equations are solved for a given velocity and density profile to yield a dispersion relation relating the complex frequency, ω , and wavenumber, k , of the oscillations. The key output of their analysis is the temporal growthrate of the absolute instability, $\omega_{0,i}$. Assuming a simplified model where the velocity and density exhibit "top hat" spatial profiles, jumping discontinuously between outer flow and wake values, they show that the dispersion relation is a function of density ratio between the outer flow and wake¹, and the ratio of reverse flow velocity in the wake to outer flow velocity, β , defined below:

$$\beta = -\frac{u(y=0)}{u(y=\infty)} \quad (3)$$

Note that the backflow ratio used in this study is related to the Λ parameter in Yu and Monkewitz [21] by

$$\beta = \frac{\Lambda + 1}{\Lambda - 1} \quad (4)$$

This leads to the following dispersion relation:

¹ For the fuel/air mixtures tested in this study, the density ratio is quite close to the temperature ratio, because the pressure and molecular weight of reactants and products is almost the same. For example, the average molecular weight changes from 27.90 to 27.88 kg/kmol from reactants to products.

$$\frac{\rho(y=0)}{\rho(y=\infty)} \left[\frac{1 + \left(\frac{\beta + 1}{\beta - 1} \right) - \frac{\omega}{k}}{1 - \left(\frac{\beta + 1}{\beta - 1} \right) - \frac{\omega}{k}} \right]^2 = -\frac{e^k + se^{-k}}{e^k - se^{-k}} \quad (5)$$

where $s = +1$ for the sinuous mode and -1 for a varicose mode. For the purpose of this study, only the sinuous mode is plotted, as it is more easily destabilized in wakes than the varicose mode. The resulting convective/absolute stability boundary is plotted in Figure 2. This figure shows that absolute instability is promoted with lower density ratios, ρ_u/ρ_b , and higher wake reverse flow velocities. In other words, as the reverse flow velocity in the wake increases, the flow becomes more absolutely unstable.

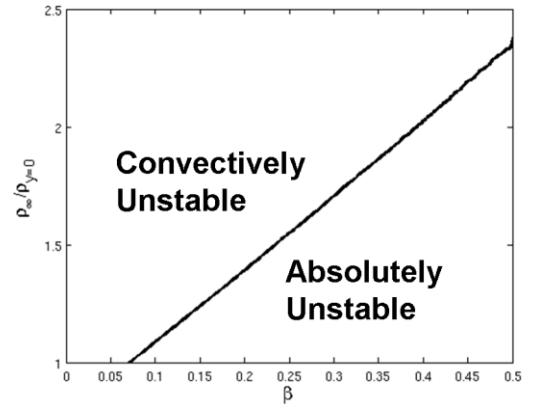


Figure 2. Dependence of convective/absolute stability limit upon backflow and density ratio, as predicted by 2D parallel flow stability analysis

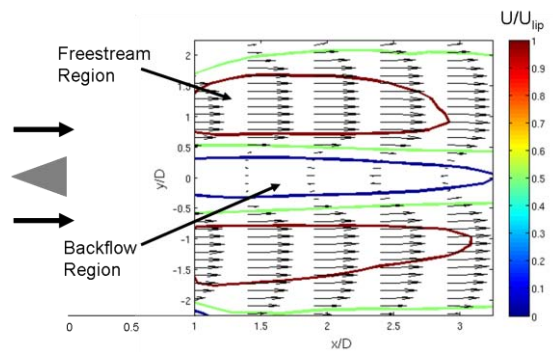


Figure 3. Illustration of the bluff body flowfield, showing region of reverse flow in the wake centerline (ballistic bluff body at 50 m/s, $\rho_u/\rho_b = 1.7$)

Computations demonstrating this same effect in combusting flows have also been presented by Erickson *et al.* [22]. Their results show that the Von Karman instability magnitude gradually grows in prominence as density ratio across the flame

is decreased below values of approximately 2-3. This observation is quite significant as it shows that the dominant fluid mechanics in a lab scale burner with non preheated reactants, which have a “high” density ratio, can be very different from that of a facility with highly preheated reactants, such as when the reactants have been adiabatically compressed to a high pressure ratio, have been preheated with a regenerative heat exchanger, or have been partially vitiated. Similarly, other experiments have clearly shown that the BVK instability becomes prominent either at low flame density ratios [23-24] or for flames close to blowoff [23, 25].

The objectives of this study are two fold. The first objective is to characterize the unsteady flow evolution as the flame density ratio is monotonically varied across this bifurcation in flow structure. While other experimental studies have clearly demonstrated the structural flow change at high and low density ratios, there does not yet appear to be a study where density ratio is systematically varied, particularly while keeping other key flow parameters such as flow velocity constant. The second objective is to compare the empirical results to the results of parallel stability theory and determine whether the transition in flow structure can be parameterized in the way suggested by theory; in particular, to determine if the density and backflow ratios have the same measured effect as theory would suggest they do. Results pertaining to the first objective are detailed in a companion paper [1] and summarized here in the Results- Flame and Flow Dynamics section. This paper focuses on detailed comparisons of these results with parallel stability theory.

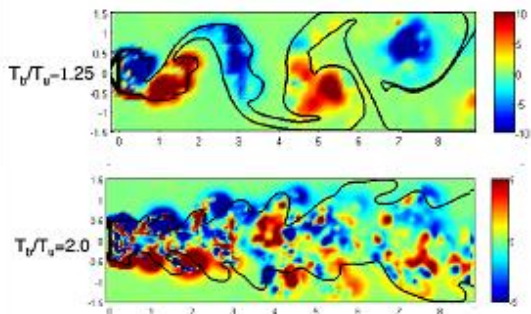


Figure 4. Computationally predicted vorticity field and instantaneous flame edge for various flame temperature ratios, reproduced from Erickson [22]

EXPERIMENTAL FACILITY, DIAGNOSTICS, AND TESTING PROCEDURES

The experimental rig, shown in Figure 5, consists of two premixed, methane-air combustors in series. The first combustor is swirl stabilized and used to vitiating the flow. The

bluff body stabilized combustor section consists of a rectangular section with a bluff body spanning the width of the combustor, creating a nominally 2D flow. The aspect ratio of bluff body height to chamber width is 0.15. This combustor has quartz windows for optical access from all four sides. Two different bluff bodies were used in the test section: a 2D ballistic shape (shown in Figure 7a), and a V-gutter (shown in Figure 7b). From here on, the 2D ballistic shape will be referred to as the ballistic bluff body.

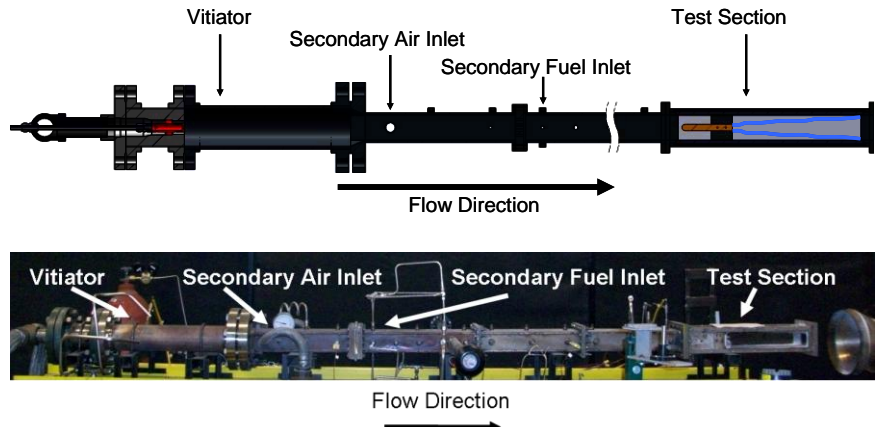


Figure 5. Schematic and photograph of the atmospheric pressure, vitiated bluff body rig

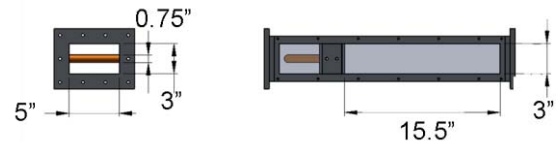


Figure 6. Schematic of test section with ballistic bluff body installed

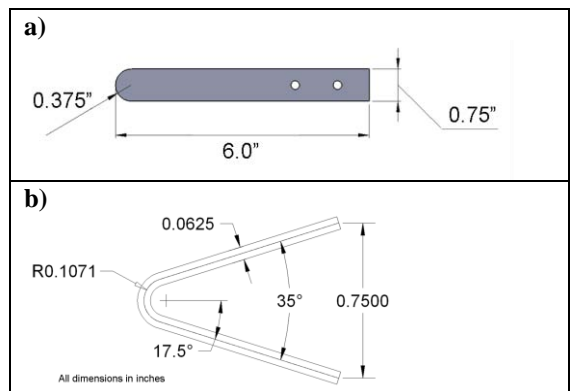


Figure 7. Schematics of bluff bodies, a) ballistic, b) V gutter

Main (primary) air and fuel were premixed upstream of the vitiator. Secondary air and fuel were plumbed into the rig and

premixed in a long settling section aft of the vitiator but upstream of the test section. The primary and secondary air and fuel each have their flowrates adjusted individually. This design allows the flame density ratio and bluff body lip velocity to be varied independently in the test section, by adjusting the air flowrate and stoichiometry in the vitiator and test section separately. The test matrix was developed such that primary and secondary air flowrates and equivalence ratios could be adjusted to achieve a specified density ratio at a fixed velocity. This test matrix design was performed using an equilibrium gas solver. A more detailed explanation of the experimental facility and the diagnostics used are provided in the companion paper [1].

Bluff body lip velocity was calculated as $U_{lip} = \dot{m} / (\rho_{lip} A_{lip})$. For this lip velocity calculation, the total measured mass flowrate and the flow cross sectional area at the bluff body trailing edge were used. The density for the lip velocity calculation was determined from the temperature measured just before the test section, assuming a gas composition of secondary air and fuel adiabatically mixed with equilibrium vitiated gas. For PIV tests a reference velocity (U_{ref}) was determined directly from the PIV velocity field as the time-averaged axial velocity just aft of the bluff body, located transversely in the center of the bulk flow.

Test matrix design was motivated by Figure 2. Actual conditions tested are provided in Figure 8, where the maximum backflow ratio β_{max} was determined from the maximum reverse flow velocity, and overlaid on the absolute stability map from Figure 2. Note that the ballistic bluff body provides a lower maximum backflow ratio than the V-gutter. Contours of constant $\omega_{0,i} D / U_{ref}$ (corresponding to the temporal growth rate of the absolute instability) are provided as well. Note that these are theoretical values that are deduced from assumptions of tophat density and velocity profiles and inviscid flow; more complex hyperbolic tangent profiles have been investigated by Monkewitz [26].

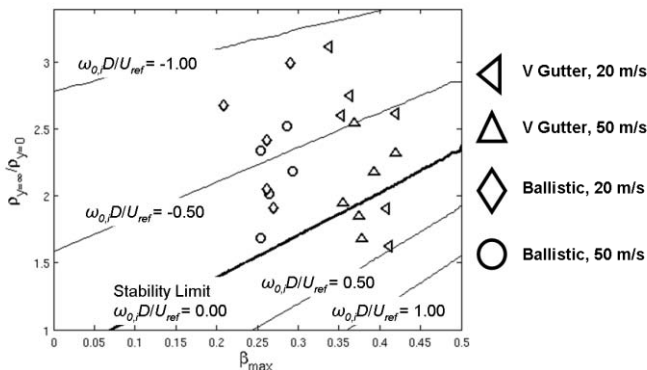


Figure 8. Tested conditions overlaid onto map obtained from 2D parallel flow stability analysis

Results were obtained for lip velocities of 20 and 50 m/s, corresponding to Reynolds number ranges from 8,000 to

20,000, based upon reactant temperature. Note that these Reynolds numbers are much lower than they would be with cold reactants because of the high viscosities associated with the vitiated reactants.

Finally, care was taken to ensure that no data were measured near blowoff boundaries, or when thermo-acoustic instabilities were present.

RESULTS - FLAME AND FLOW DYNAMICS

This section summarizes key results from Ref. [1] on the time series and spectra of both flame and flow dynamics as a function of flame density ratio. These results will be heavily utilized in the “Comparisons with Parallel Stability Analysis” section.

SPECTRAL AND CORRELATION ANALYSIS

Representative results are presented here for the flame and flow dynamics. Flame dynamics, measured by high speed video, were quantified via the transverse position of the top and bottom flame branch edges, $\zeta_U(x,t)$ and $\zeta_L(x,t)$, as a function of axial position and time (see Figure 9). This resulted in time series for edge positions along both flame branches, at each axial position. These time series are Fourier transformed to determine their temporal spectra, given by $\zeta_U(x,f)$ and $\zeta_L(x,f)$.

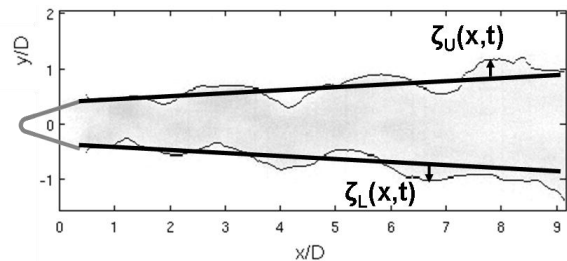


Figure 9. Coordinate system and instantaneous flame edge position definition from edge tracking, 50 m/s, $\rho_u/\rho_b = 1.7$.

PIV data were used for corresponding analysis of flowfield dynamics. A sample time-averaged velocity field from PIV is presented in Figure 3 from the ballistic bluff body at 50 m/s, $\rho_u/\rho_b = 1.7$. Unsteady PIV data shown in this section were analyzed by observing the transverse centerline velocity $v'(x,y=0,t)$ and, after taking a Fourier transform, its temporal spectrum $v'(x,y=0,f)$.

Figure 10a shows spectra from the upper flame branch at $x/D=3.5$ at three different density ratios as a function of Strouhal number, $St_D = fD/U_{lip}$. Although not shown, spectra for the V-gutter tests were qualitatively similar. At the highest density ratio shown, $\rho_u/\rho_b=2.4$, the spectrum is fairly evenly distributed across all frequencies, with a small bump at $St_D \sim 0.24$. As the density ratio is decreased to 2.0, a clear feature appears centered near $St_D = 0.25$. As the density ratio is further decreased to 1.7, the response at $St_D = 0.25$ becomes very

narrowband and quite prominent. Figure 10b shows spectra of the unsteady transverse velocity for the same flow conditions, and demonstrates that the flow similarly exhibits a growing narrowband spectral feature at $St_D=0.25$.

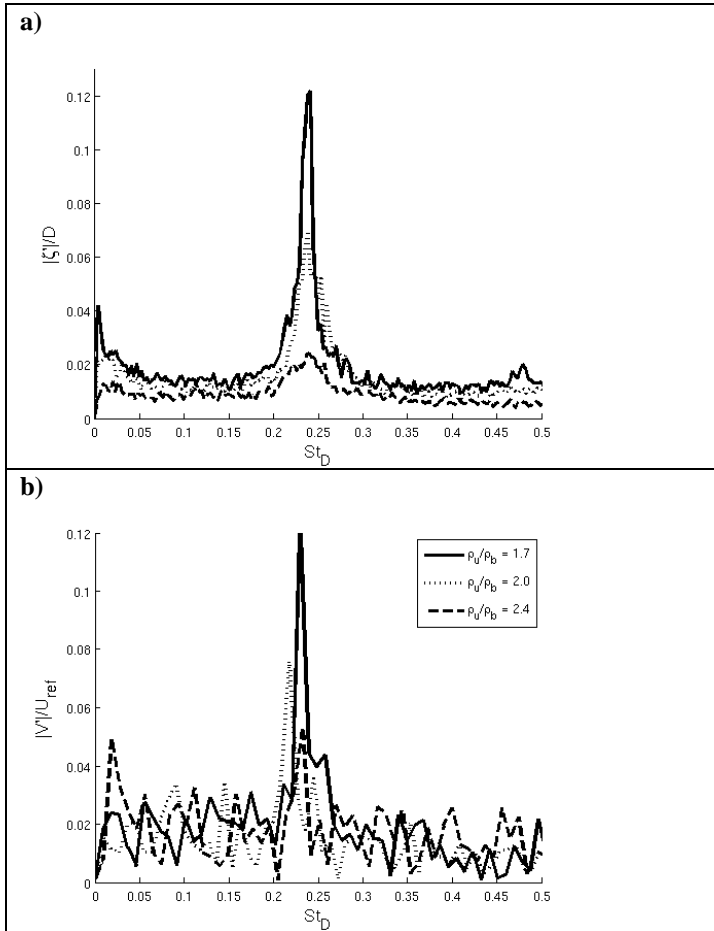


Figure 10. Spectra for ballistic bluff body at 50 m/s and $x/D = 3.5$ for a) upper flame edge and b) centerline transverse unsteady velocity magnitude.

These spectral peaks are due to a hydrodynamic, as opposed to an acoustic disturbance, as manifested by the fact that they appear at roughly the same Strouhal number (~ 0.24) at both flow velocities and across the range of density ratios.

In order to focus on the characteristics of this response near the frequency of peak response, the integrated power under the spectral peak between $0.20 < St_D < 0.28$ as a function of density ratio is computed for the flame response spectra in Figure 10a, and for the unsteady transverse velocity spectra in Figure 10b. This power is converted to a root mean square (RMS) of the signal at the response frequency by use of Parseval's theorem, using the relation below that relates RMS of the time series $s(t)$ of duration T and spectrum $\hat{s}(f)$,

$$s_{rms} = \sqrt{\frac{1}{T} \int_{f^-}^{f^+} |\hat{s}(f)|^2 df} \quad (6)$$

These RMS values are presented in Figure 11 for both the flame and the flow. The flame data in Figure 11 show that the normalized fluctuation in flame position has a value of roughly 6% over the $2.4 < \rho_u/\rho_b < 3.4$ range. Below a value of $\rho_u/\rho_b = 2.4$, the response gradually increases to 20% at $\rho_u/\rho_b = 1.7$. Comparing the flame to the flow data again demonstrates similarities. This plot also indicates that the transition in flow and flame characteristics is not an abrupt bifurcation with change in density ratio, but a more gradual increase in narrowband response as the density ratio decreases.

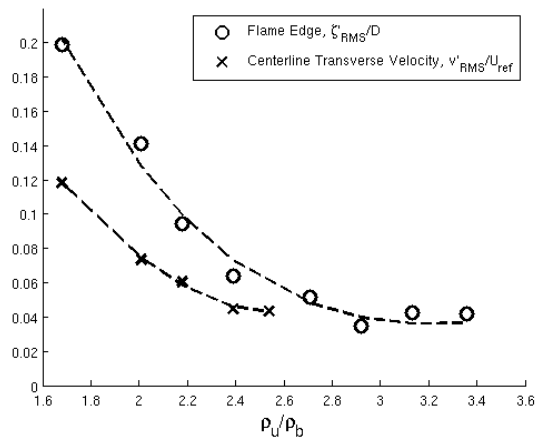


Figure 11. Dependence of spectral energy upon density ratio for ballistic bluff body at 50 m/s and $x/D = 3.5$, expressed as RMS flame edge fluctuation averaged over both flame branches, and RMS centerline transverse unsteady velocity.

The correlation coefficient between the two flame branches, $\rho_{U,L}$ (defined below), provides important information on the scale and/or correlation between the underlying flow structures perturbing them.

$$\rho_{U,L}(x) = \frac{\langle \xi_U(x,t) \xi_L(x,t) \rangle}{\sqrt{\langle (\xi_U(x,t))^2 \rangle \langle (\xi_L(x,t))^2 \rangle}} \quad (7)$$

Note that negative and positive correlation coefficients mean an asymmetric and symmetric flame disturbance, respectively. Furthermore, a near zero correlation coefficient implies that the flame is disturbed by uncorrelated structures much smaller than their transverse separation distance, roughly the bluff body diameter.

Although not shown, calculations of the dependence of correlation coefficient upon ρ_u/ρ_b show that the correlation coefficients are near zero for $\rho_u/\rho_b > \sim 2.5$. The correlation

coefficient monotonically decreases towards values of $\rho_{U,L} \sim 0.6$, indicative of *growing correlation* and *asymmetric motion* with decreasing flame density ratio.

These results show that there is a gradual increase in spectral energy at $St_D=0.24$, with a corresponding increase in asymmetry and large scale structures in the wake with decreasing ρ_u/ρ_b . The very narrowband spectral nature of the flow in Figure 10 suggests that the flow evolves to a limit-cycling, absolutely unstable flow at low density ratios. These data also suggest that the limit cycle amplitude of the absolutely unstable flow oscillator grows monotonically in amplitude with decreases in density ratio for $\rho_u/\rho_b < 2.4$.

INTERMITTENCY

The above measures of the flame structures are averaged temporal attributes and ignore the fact that the flame dynamics are actually highly intermittent in time. As will be shown next, it appears that rather than characterizing the limit cycle amplitude as monotonically growing in amplitude with ρ_u/ρ_b , a better description is that the flow has two possible states and intermittently flips between them. The relative fraction of time the flow spends in each state monotonically varies with density ratio. This intermittent character is evident from Figure 12, which shows two images of the flame at the *same operating conditions, but different instances of time*.

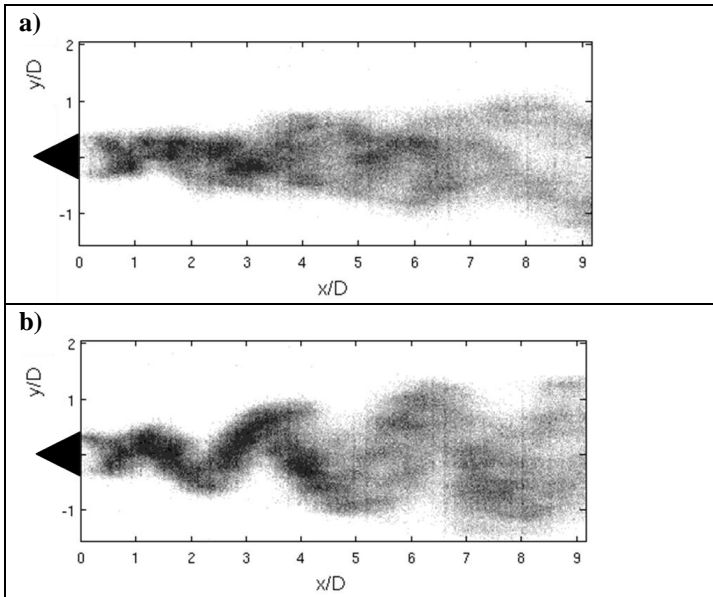


Figure 12. Intermittent wake structure evident in two flame images from the same high speed video for ballistic bluff body at 50 m/s, $\rho_u/\rho_b = 1.7$

In order to quantify intermittency, the time series were locally fit to a sinusoidal fluctuation with a fixed frequency of $f_o=0.24U_{tip}/D$ ($\sim 630\text{Hz}$ at 50 m/s) over a two period window. Within each window a correlation coefficient, ρ_f (defined below), was calculated between the sine fit and the actual data, providing a measure of the goodness of fit.

$$\rho_f(x) = \frac{\langle \zeta_U(x,t) \sin(2\pi f_o t) \rangle}{\sqrt{\langle (\zeta_U(x,t))^2 \rangle \langle (\sin(2\pi f_o t))^2 \rangle}} \quad (8)$$

A sample plot of the temporal dependence of ρ_f at $\rho_u/\rho_b = 1.7$ is plotted in Figure 13, illustrating that it spends a significant fraction of time between 0.9-1.0 for flame edge position (slightly less for velocity), but also has certain periods of time where it drops to values well below 0.5.

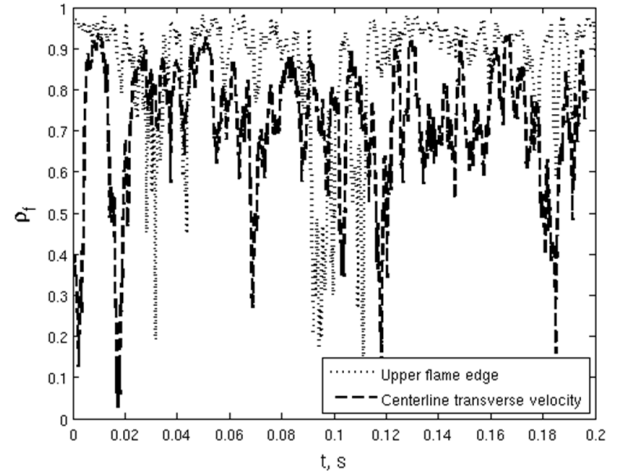


Figure 13. Correlation coefficient between sine fit and time signal for ballistic bluff body at 50 m/s, $x/D = 3.5$, $\rho_u/\rho_b = 1.7$, for a) upper flame edge and b) centerline transverse unsteady velocity

The fraction of time that this correlation coefficient exceeds a specified threshold value, ρ_t , was then computed at each spatial location and density ratio. Figure 14 plots a typical result at two threshold values. Notice the similarities between the spectral energy plot, Figure 11, and the intermittency plot, Figure 14.

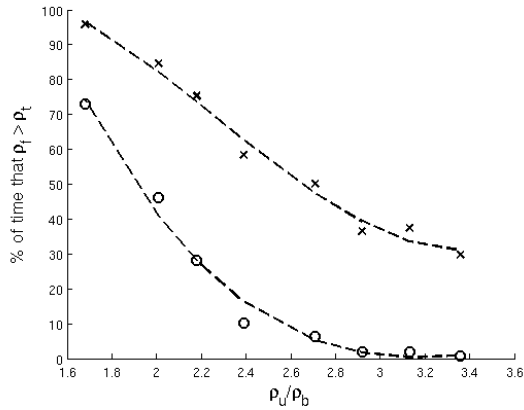


Figure 14. Percent of time that sine fit correlation coefficient for upper flame edge position is greater than the threshold value for ballistic bluff body at 50 m/s, $x/D = 3.5$. Results for two threshold values are presented with symbol x for $\rho_t = 0.5$ and symbol o for $\rho_t = 0.8$.

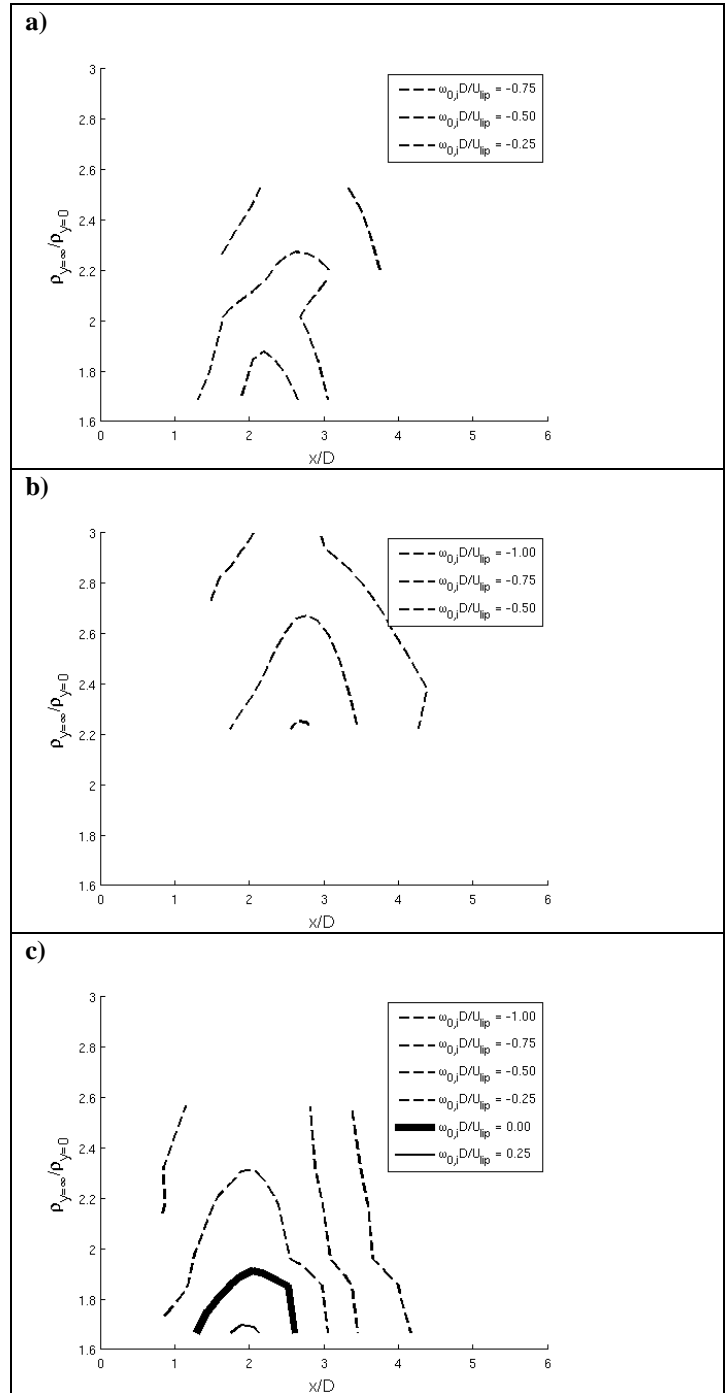
Although not shown for reasons of space, results at other spatial locations indicate qualitatively similar results. The fraction of time that the flow spends in the “periodic state” monotonically grows with downstream distance. These data clearly support the notion that the rise in narrowband energy is associated with both an increased fraction of time that the flow spends in a limit-cycling state, manifested by asymmetric structures with length scales of the order of the bluff body diameter, and an increase in limit cycle amplitude of absolutely unstable flow [1].

COMPARISONS WITH PARALLEL STABILITY ANALYSIS

This section compares and correlates several of the above described data characteristics to predictions from the locally parallel stability analysis sketched out in the Introduction. In order to plot the experimental tests on the stability map shown in Figure 2, knowledge of the backflow ratio and density ratio was required for each condition. The axial velocity fields obtained from PIV data were used to calculate the velocities needed to quantify the backflow ratio, $\beta(x)$. The velocity information needed to calculate β was determined from the axial velocity on the centerline and the freestream velocity (see Figure 3 for illustration).

Stability predictions of $\omega_{0,i}D/U_{lip}$ (the normalized temporal growth rate of the absolute instability) as a function of axial position are presented next. Figure 15 plots calculated instability growth rate contours as functions of axial position and density ratio for both bluff bodies at lip velocities of 50 m/s and 20 m/s. Regions of positive absolute instability growthrate, $\omega_{0,i}D/U_{lip} > 0$, indicate the presence of absolute instability. This occurs at sufficiently low density ratios at axial positions roughly two bluff body diameters downstream. The spatial extent of these absolute instability pockets grows with

decreasing density ratio. Note that the absolute instability region does not start immediately aft of the bluff body, because of the low backflow velocities immediately downstream of the bluff body.



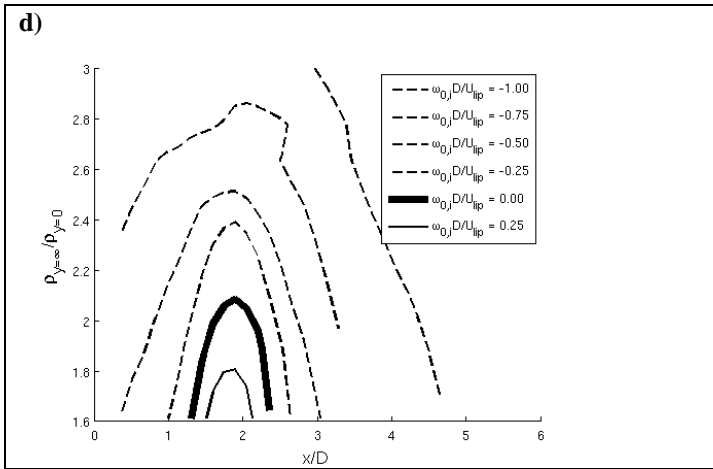


Figure 15. $\omega_{0,i} D/U_{lip}$ contour maps vs axial position and density ratio, for a) ballistic bluff body at 50 m/s, b) ballistic bluff body at 20 m/s, c) V-gutter at 50 m/s, d) V-gutter at 20 m/s

We next consider the measured axial dependence of the centerline velocity fluctuations at $St_D = 0.24$ and compare these profiles to predicted absolute instability regions. In order to overlay results from different conditions, the axial coordinate is referenced to the location of maximum absolute instability growth rate, x_{AI} (obtained from Figure 15), which corresponds to the location of maximum reverse velocity. These plots are presented in Figure 16.

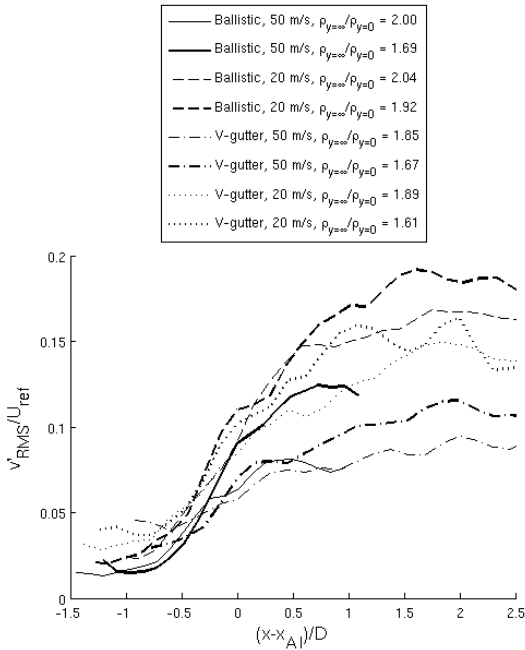


Figure 16. v'_{RMS} vs distance downstream from the predicted location of maximum absolute instability growthrate for several test conditions

Figure 16 shows that growth of the narrowband $St_D \sim 0.24$ fluctuations begins at approximately the same referenced location. Once it has grown in the region of absolute instability, the structure associated with this mode may continue to be amplified as it passes through the downstream convectively unstable regime. This reinforces the idea that the wake mode characterized by large-scale, asymmetric vortex shedding is triggered by a pocket of absolute hydrodynamic instability in the wake whose location is predicted by local parallel stability analysis.

The above results have focused on comparison of local attributes of the data with the local stability theory. However, such a comparison is complicated by the fact that no clearcut bifurcation was observed. Rather, the wake structure is highly intermittent, with a degree of intermittency that gradually transitions from one flow state to another with change in density ratio.

In order to compare the stability characteristics of the different geometries and velocities, Figure 17 summarizes the data by plotting the maximum $\omega_{0,i} D/U_{lip}$ for a given test (corresponding to β_{max}) as a function of the intermittency factor. Intermittency is quantified by the fraction of time that $\rho_j > \rho_l = 0.5$. The figure shows that there is a good correlation between absolute instability growth and intermittency. Moreover, the slopes of all four data sets are quite comparable. It is also evident that absolute instability values are systematically lower with the ballistic shape than the V-gutter.

We hypothesize that intermittency is associated with the fact this flow is at a relatively high Reynolds number, so that no sharp bifurcation in flow characteristics occurs. It should be emphasized that the parallel stability analysis assumes a “quiescent” base state; i.e., one without turbulent fluctuations. Nonetheless, the variation in intermittent characteristics of the flow is well correlated by the absolute stability characteristics of a quiescent base state flow with similar mean flow properties.

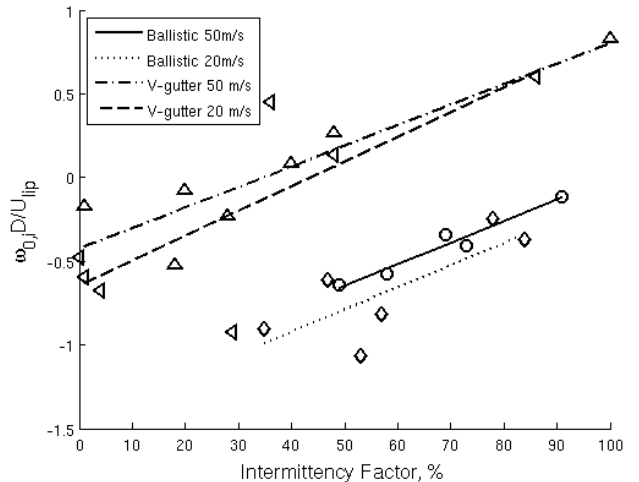


Figure 17. Dependence of predicted growth rate upon measured intermittency factor.

CONCLUDING REMARKS

Results from parallel flow stability analysis were used to correlate various measured features of a reacting bluff body wake. This information was used to show that the wake's large-scale sinuous motion, if it exists, spawns at a location near the maximum absolute instability growthrate. Additionally, this study shows that the wake mode intermittency is correlated with the maximum growthrate of absolute instability in the wake. It is also encouraging that this result was obtained with such a significantly simplified model. The next step in improving the stability model is to derive a dispersion relation for a more accurate wake velocity profile.

These results emphasize that the convective/absolute instability transition does not occur abruptly at a certain ρ_u/ρ_b value for the high Reynolds number flow considered here. This has important implications on high Reynolds number vitiated flows, many of which operate in the transitional, highly intermittent density range. This suggests that such flows intrinsically operate in two co-existing dynamical states, intermittently jumping between the two. An important future study is to characterize the effects of narrowband acoustic excitation on these flow structures. While the effect of such excitation on a convectively or absolutely unstable flow is reasonably well understood (see Introduction), its effect in this highly intermittent flow will require clarification.

REFERENCES

1. Emerson, B., et al., *Dependence of the Bluff Body Wake Structure on Flame Temperature Ratio*, in *49th AIAA Aerospace Sciences Meeting including the New Horizons Forum and Aerospace Exposition*. 2011: Orlando, Florida.
2. Shanbhogue, S.J., S. Husain, and T. Lieuwen, *Lean blowoff of bluff body stabilized flames: Scaling and dynamics*. *Progress in Energy and Combustion Science*, 2009. **35**(1): p. 98-120.
3. Criminale, W.O., T.L. Jackson, and R.D. Joslin, *Theory and Computation in Hydrodynamic Stability*. 2003, Cambridge: The Press Syndicate of the University of Cambridge.
4. Godreche, C. and P. Manneville, *Hydrodynamics and Nonlinear Instabilities*. 1998, Cambridge: University Press, Cambridge.
5. Schmid, P.J. and D.S. Henningson, *Stability and Transition in Shear Flows*. 2001, New York: Springer.
6. Anderson, K.R., J. Hertzberg, and S. Mahalingam, *Classification of Absolute and Convective Instabilities in Premixed Bluff Body Stabilized Flames*. *Combustion Science and Technology*, 1996. **112**(1): p. 257-269.
7. Huerre, P. and P.A. Monkewitz, *Local and global instabilities in spatially developing flows*. *Annual Review of Fluid Mechanics*, 1990. **22**(1): p. 473-537.
8. Ho, C.-M. and P. Huerre, *Perturbed Free Shear Layers*. 1984, University of Southern California: Los Angeles.
9. Masselin, M. and C.-M. Ho, *Lock-On and Instability in a Flat Plate Wake*, in *AIAA Shear Flow Control Conference*. 1985: Boulder, CO.
10. Blevins, R.D., *Flow-Induced Vibration*. 1977, New York: Van Nostrand Reinhold Co.
11. Cardell, G.S., *Flow past a circular cylinder with a permeable splitter plate*. 1993, California Institute of Technology: Pasadena.
12. Prasad, A. and C.H.K. Williamson, *The Instability of the Shear Layer Separating from a Bluff Body*. *Journal of Fluid Mechanics*, 1997. **333**: p. 375-402.
13. Perry, A.E., M.S. Chong, and T.T. Lim, *The vortex shedding process behind two-dimensional bluff bodies*. *Journal of Fluid Mechanics*, 1982. **116**: p. 77-90.
14. Cantwell, B. and D. Coles, *An experimental study of entrainment and transport in the turbulent near wake of a circular cylinder*. *Journal of Fluid Mechanics*, 1983. **136**: p. 321-374.
15. Bearman, P., *On vortex shedding from a circular cylinder in the critical Reynolds number regime*. *J. Fluid Mech*, 1969. **37**: p. 577.
16. Roshko, A., *Experiments on the flow past a cylinder at very high Reynolds numbers*. *Journal of Fluid Mechanics*, 1961. **10**: p. 345-356.
17. Roshko, A., *On the Wake and Drag of Bluff Bodies*. *Journal of the Aeronautical Sciences*, 1955. **22**(2): p. 124-132.
18. Huang, R.F. and K.T. Chang, *Oscillation Frequency in Wake of a Vee Gutter*. *Journal of Propulsion and Power*, 2004. **20**(5): p. 871-878.
19. Roshko, A., *On the drag and shedding frequency of two-dimensional bluff bodies*. 1954, National Advisory Committee on Aeronautics.
20. Zdravkovich, M.M., *Flow Around Circular Cylinders: A Comprehensive Guide Through Flow Phenomena, Experiments, Applications, Mathematical Models, and Computer Simulations*. 1997: Oxford University Press.
21. Yu, M.-H. and P.A. Monkewitz, *The effect of nonuniform density on the absolute instability of two-dimensional inertial jets and wakes*. *Phys. Fluids*, 1990. **2**(7).
22. Erickson, R.R., M.C. Soteriou, and P.G. Mehta, *The Influence of Temperature Ratio on the Dynamics of Bluff Body Stabilized Flames*, in *44th AIAA Aerospace Sciences Meeting & Exhibit*. 2006: Reno, Nevada.
23. Kiel, B., et al., *Non-Reacting and Combusting Flow Investigation of Bluff Bodies in Cross Flow*, in *42nd AIAA/ASME/SAE/ASEE Joint Propulsion Conference & Exhibit*. 2006: Sacramento, California.

24. Cross, C., et al., *Dynamics of Non-Premixed Bluff Body-Stabilized Flames in Heated Air Flow*, in *ASME Turbo Expo*. 2010: Glasgow, UK.
25. Kiel, B., et al., *A Detailed Investigation of Bluff Body Stabilized Flames*, in *45th AIAA Aerospace Sciences Meeting & Exhibit*. 2007: Reno, Nevada.
26. Monkewitz, P.A., *The absolute and convective nature of instability in two-dimensional wakes at low Reynolds numbers*. 1988, Department of Mechanical, Aerospace, and Nuclear Engineering: Los Angeles, CA.